

Research Article

Fracture Development and Multifield Coupling Evolution Law of Soft Overburden Rock in a Medium-Thick Coal Seam Mine

Junjie Cai ¹, Xijian Li ¹, Longxing Guo,² Haiteng Xue,³ and Bize Xu⁴

¹Mining College, Guizhou University, Guiyang 550025, China

²Coal Science and Technology Research Institute Co. Ltd., Beijing 100020, China

³School of Emergency Management and Safety Engineering, China University of Mining and Technology Beijing, Beijing 102206, China

⁴Taizhou Special Equipment Inspection and Testing Institute, Taizhou 318000, China

Correspondence should be addressed to Xijian Li; xjli1@gzu.edu.cn

Received 30 December 2021; Accepted 24 February 2022; Published 23 March 2022

Academic Editor: Xiangguo Kong

Copyright © 2022 Junjie Cai et al. This is an open access article distributed under the Creative Commons Attribution License, which permits unrestricted use, distribution, and reproduction in any medium, provided the original work is properly cited.

To study the fracture development and multifield coupling evolution law of soft overburden rock for medium-thick coal seam mining, taking the first 50105 working face of the Faer coal mine as the research background, a numerical simulation, a fractal theoretical analysis, and network parallel electric method experiments were conducted; the fracture development and coupled stress field and energy field evolution law of soft overburden rock for medium-thick coal seam mining are analyzed. The results showed that the overburden collapse process could be divided into three stages: pseudo-top collapse to key layer breakage, key layer breakage to overburden bending, and overburden bending to collapse and compaction. The fractal dimensions of the overburden fracture before and after breakage of the key layer showed a rising-stable-declining trend, and the experimental analysis showed that fracture development began in the unmined area at the front end of the working face under the influence of overstress. In addition, the height of fracture development after stabilization was 53.7 m. A relationship was established between the height of the overburden fracture, peak stress, and dissipation of the energy density of the key layer, and their associated disaster mechanism induced by mining in a medium-thick coal seam progressed as follows: coal mining → stress redistribution → dissipation energy increase → fracture development → stress concentration → key stratum breaking → stress transfer → energy release → dynamic disaster. These results can be used as a reference for observing and mastering the development law of overburden fractures and preventing disasters under such conditions.

1. Introduction

The mining area in southwest China has certain geological characteristics, such as a shallow burial depth, thin bedrock, a medium-thick coal seam, and soft overburden lithology. High-intensity mining methods are prone to causing the movement and breakage of overburden rock, which generates large numbers of fissures that affect the transport of groundwater, the flow of gas, and the settlement and movement of surface rock strata, in addition to seriously jeopardizing safe production in the coal mines [1, 2]. Therefore, to ensure safe coal mining, it is necessary to analyze the overburden fissure development law and associated

disaster-causing mechanisms in medium-thick coal seam mines [3].

Many studies have extensively researched the development law of mining-induced overburden fractures. For example, Li et al. [4] studied the deformation characteristics of the overburden in shallow and extrathick coal seams using full-perspective borehole photography and seismic CT scanning technology. They determined the height of the overburden fault zone, and their results could be used as a theoretical basis for controlling the overburden in a shallow roofed mine. Wang et al. [5] studied the role of the overburden roof in the mining of extrathick coal seams with deep long arms and found that continuous fracture of the roof

increased the support stress and strain of the coal seam, which could result in dynamic disasters such as rockbursts. In addition, Yang et al. [6] determined that the roof rock height and fault zone in the subsidence area of extrathick coal seams mainly comprised key layers that underwent obvious and combined deformation, subsidence, and failure. Lan et al. [7] found that cantilever beams, top beams, and high-rise structures were formed after mining extrathick hard-top coal seams, and these events were unique to large-space mining sites. Furthermore, Zhang et al. [8] proposed a space-space-ground (3S) integrated system to understand the overburden transportation mode under the mining of extrathick coal seams.

Du and Gao [9] used numerical simulations to study the development of the hydraulic fault zone in the longwall mining of thick coal seams, and the results showed that under the same stratum conditions, the mining method employed has a great influence on the height of the hydraulic fault zone. Mondal et al. [10] calculated the fractal dimension “ D_c ” from microseismic data, both to monitor the state of the overlying rock layers and for spatial and temporal prediction of roof collapse. Liang et al. [11] conducted similar material simulation experiments for thick coal seams and concluded that the fractal dimension of the horizontal and vertical zones of the mining fracture network with the mining progress and different mining feeds has self-similar characteristics, and the fractal dimension distribution of the mining fractures has a general “W”-type trend. Wu et al. [12] studied the overburden movement of a thick coal seam using similar simulation experiments. Before the crushing of thick argillite, the developmental height of the overburden peel developed nonlinearly upwards with the advancement of the working face, and the developmental height after crushing was blocked by the thick argillite. Chen et al. [13] proposed a calculation method based on the fracture mechanics analysis of soft and hard rock strata and determined the failure height of a thick coal seam overburden. Through field experimental analysis, the fracture section of soft rock strata was found to have no obvious fracture, and the fracture width of the hard rock strata was greater than that of the soft rock. Based on a numerical simulation of consolidation in the subsidence area and tensile failure in the fault area, Shu et al. [14] reported that the tensile fracture strength in the fault area of a thick coal seam had a significant influence on the distribution of mining stress and the rock layer. In addition, Xu et al. [15] studied the influence of the thick coal seam mining overburden on loose aquifers and showed that coal seam excavation reduced the impermeability of the aquifer and increased the hydraulic gradient between the porous aquifer and fractured bedrock aquifer. Ma et al. [16] introduced fault fractal dimensions and fold fractal dimensions as indicators of aquifer permeability, and after a fuzzy comprehensive evaluation, permeability levels were delineated in the study area of thick coal seams. Li et al. [17] determined that with the advancement of the shallow thick coal seam working face, the key load-bearing layer broke, the overburden moved as a whole, and various surface cracks, mainly tensional ones, appearing on the surface lagging behind the working face. Hu et al. [18] used the Brillouin optical time-domain reflec-

tion method to regularly monitor the fiber strain in a thick coal seam overburden; they obtained the distribution characteristics of the fiber strain, its maximum height, and its law of evolution in a water-conducting fault zone. In addition, Liu et al. [19] used various research methods to study the overburden movement of a thick coal seam and determined that coal seam separation and collapse underwent a process of stepped or leap-forward development. Through obtaining actual measurements, He et al. [20] found through that under certain geological engineering conditions, such as increasing the propulsion speed, reducing the mining height, or shortening the width of the panel, the degree of overburden damage was weakened in a thick coal seam. Yuan et al. [21] used distributed optical fiber sensing monitoring to reveal the spatiotemporal evolution of a thick coal seam, and Yang et al. [22] used the fractal dimension and stress distribution to quantitatively describe the development of overburden faults during thick coal seam mining. Furthermore, Wang et al. [23] found that the calculation results from a numerical model were basically consistent with those of a theoretical analysis, and the height of the fractured water diversion zone of the thick coal seam was approximately 1.5 times that of the nonfractured water diversion zone. Du et al. [24] monitored and studied mining-driven overlying change patterns in shallow and thick coal seams by embedding distributed fiber and fiber grating sensors in physically similar model species. Cheng et al. [25] believed that the development of fault zones in thick coal seam overburden was greatly affected by mining, and the connected fault zones had a “trapezoidal platform structure.”

The above studies have mostly focused on the development of mining fissures in extrathick coal seams and thick coal seams, but few studies have focused on such occurrences in medium-thick coal seams. The coal seam in the first mining face of 50105 in the Faer coal mine has an average thickness of 1.91 m. It has an average mining width and burial depth of 145 m and 173 m, respectively, and the top plate of the coal seam in this area is mostly mudstone or siltstone. The thick coal seam in the 50105 mining face thus has a weak rock face. Based on the actual mining conditions in the Faer coal mine, discrete element software was used to model fracture development and the network parallel electrical method was used to research the rule of overburden rock fracture development. In addition, the fractal dimension was calculated and the fracture field and stress field were determined. The relationship between these parameters (such as the energy field) was analyzed, and the coupling evolution laws of the mining-induced fracture field, stress field, and energy field were determined.

2. Project Background

The Faer coal mine is located in the south of Liupanshui City within Guizhou Province. The coal-bearing strata of the mine belong to the Upper Permian Longtan Formation. The 50105 working face is located in the middle of the south wing of the Wushang mining area, and it has a trend length and dip width of 674 m and 145 m, respectively. The backmining seam of the 50105 working face comprises 1 coal from the upper segment

of the Longtan Formation, and it has a dip angle of 7° – 11° (average 9°) and a gangue thickness of 0–0.7 m. The average mining height is 2.91 m, and the maximum mining height is 3 m (consolidated mining). The overlying strata have a thickness of only 16 m, and the upper part mainly comprises silty clay containing gravel. Figure 1 presents a lithologic histogram of the overlying strata.

The working face is a medium-thick coal seam at a shallow burial depth in thin bedrock with a soft overlying lithology, and the key layer is a relatively hard siltstone that has weak rock control and other geological features.

3. Numerical Simulation and Calculation of Fractal Dimension of Fracture

3.1. Numerical Simulation. The UDEC (Universal Distinct Element Code) numerical model (Figure 2) was established based on the geological conditions of the 50105 working face of the Faer coal mine. The Mohr-Coulomb criterion was adopted in the excavation simulation, and the double-yield constitutive model was applied in the gob elements. The model's dimensions were as follows: length, height, and coal seam thickness of 200 m, 100 m, and 1.9 m, respectively. The joints were divided according to the overburden lithology, and the model boundary was fixed and constrained. To reduce the left and right boundary effect, coal pillars measuring 40 m were created on both sides. The middle mining length was 120 m, and each advance distance was 10 m. The physical and mechanical parameters of each rock layer and the joints are listed in Table 1.

3.2. Calculating the Fractal Dimension of the Evolution of Overburden Fracture. Based on a two-dimensional numerical simulation, the fracture development characteristics of the overlying rock were analyzed to study the development of fractures within the target area.

The numerical simulation was used to record the overlying rock transport characteristics and their associated fracture development characteristics after each advance; then, the fracture development features were binarized by using AutoCAD (Autodesk Computer-Aided Design) and Origin. The box dimension method was subsequently employed to calculate the dimensions of the fracture network using the following processing flow: the fracture evolution diagram in the overlying rock at different advance distances was covered with a square grid on a scale of r , the number of grids containing fractures was counted and recorded as $N(r)$, and the number of non-space subdivisions $N(r)$ was recorded by constantly changing the size of r . The slope of the linear fit of the data was the fractal dimension for r , and $N(r)$ was taken as a double logarithm [26, 27]:

$$D = -\lim_{r \rightarrow 0} \frac{\lg N(r)}{\lg r}. \quad (1)$$

To calculate the box fractal dimension D , the fractal dimension code was written and programmed independently in MATLAB software, and the slit binary map was

imported to quickly calculate the fractal dimension of the 2 D digital image.

Table 2 shows the numerical simulation of the overburden transport map, the fracture binary map, and calculations of the fractal dimension of the overburden fracture at different advance distances.

The relationships between the fracture development characteristics of the overlying rock and the fractal dimensions of the fracture are shown in Table 3.

4. Study of Fracture Development Characteristics of Overburden Rock

4.1. Study of the Fractal Characteristics of Overburden Fractures before and after Breakage of the Key Layer. As the working face advances, the overlying rock layer in the mining area collapses under the action of self-gravity and horizontal stress, and it then collapses, sinks, horizontally transported, fractures, and then reforms into a balanced state. After the overlying rock layer is broken by transverse delamination and a longitudinal fracture, the overlying rock fracture gradually expands above the mining void area, thus showing dynamic development. According to the key layer breakage characteristics during the working face advancement process, the entire advancement process can be divided into the following stages: pseudo-top collapse to key layer breakage, key layer breakage to overburden rock bending, and overburden rock bending to collapse compaction stage. According to the relationship between the fractal dimension of the fracture network and the advancing distance shown in Figure 3, these three stages in detail are as follows:

- (1) In stages I and II (the period from pseudo-top collapse to key layer breakage), as shown by the white-shaded area, the fractal dimension of the fracture network increases from 1.096 to 1.139. When the working face advances from 20 m to 50 m, the relatively hard siltstone is the key breakage layer, and the lower rock layer collapses under the influence of stress, thereby forming collapse fractures. The fractal dimension undergoes an increasing trend with an increase in the excavation distance, which indicates that the fracture network undergoes dynamic development during the period from the collapse of the pseudo-top to the breakage of the key layer
- (2) In stages II and III (the period from key layer breakage to overburden bending), as shown by the orange-shaded area, the fractal dimension of the fractal network increases from 1.139 to 1.144. When the working face advances from 50 m to 80 m, debris accumulates in the quarry area as the key layer breaks, and the lower collapse feature is obvious. The lower rock layer collapses and tends to get compacted, the fractures are distributed in a step shape, and the fractures on the two legs of the trapezoid show overdevelopment phenomenon and smooth volatility


Columnar	Thickness (m)		Lithology	Series	System	Erathem
	Minimum to maximum (m)	On average (m)				
	3.0~7.4	5.20	Argillaceous siltstone	Longtan Group	Permian	Paleozoic
	2.4~4.3	3.35	Siltstone			
	2.8~5.7	4.25	Argillaceous siltstone			
	0.0~0.5	0.25	Mudstone			
	1.30~2.51	1.91	Coal seam 1#			
	0.1~0.4	0.25	Aluminum mudstone			
	7.1~11.8	9.45	Fine sandstone			

FIGURE 1: Lithological diagram of overlying rocks.

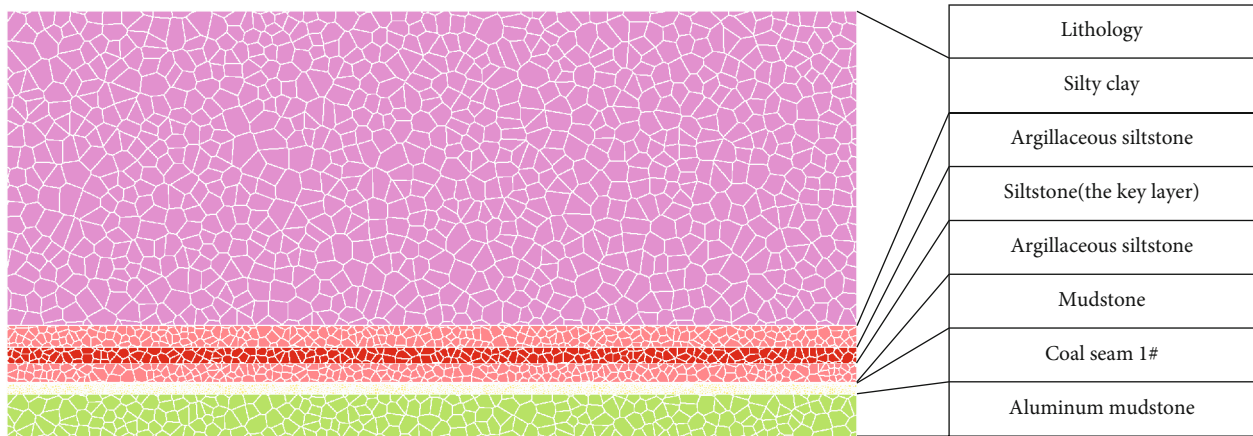


FIGURE 2: Sketch of the numerical model.

TABLE 1: Physical and mechanical parameters of coal strata.

Rock layer	Density ($\text{kg}\cdot\text{m}^{-3}$)	Bulk modulus (Gpa)	Tensile strength (MPa)	Internal cohesion (MPa)	Angle of internal friction ($^{\circ}$)
Fine sandstone	2750	29.50	2.03	3.64	39.69
1 coal	1420	34.20	1.20	0.90	20.00
Mudstone	2360	8.50	4.60	2.66	38.60
Muddy siltstone	2570	30.10	3.64	1.55	39.40
Siltstone	2760	35.90	2.42	4.20	41.20
Chalky clay	1820	0.001	0.00	0.03	23.00

(3) In stages III and IV (the period from overburden bending to collapse compaction), as shown by the blue-shaded area, the fractal dimension of the fracture network decreases from 1.144 to 1.119. As the working face advances from 80 m to 120 m, fracture development stabilizes. The top of the goaf basically touches the gangue. The silty clay in the central overburden of goaf is soft and gradually compacted by the load. Off-layer fractures occur easily as closure phenomenon. Bending and sinking of the upper powder

clay area in the model are obvious. Therefore, the fractal dimension of the fracture network can be used to reveal the fracture development of the overlying rock layer, and changes in the fractal dimension can be used to predict the fracture network development of the overlying rock layer

4.2. Analysis of Variation in Peak Stress within Overlying Rocks. In order to further analyze and study the relationship between overburden stress change and fractal

TABLE 2: Numerical simulation diagram, binary diagram, and fractional dimensional diagram associated with different working face advances.

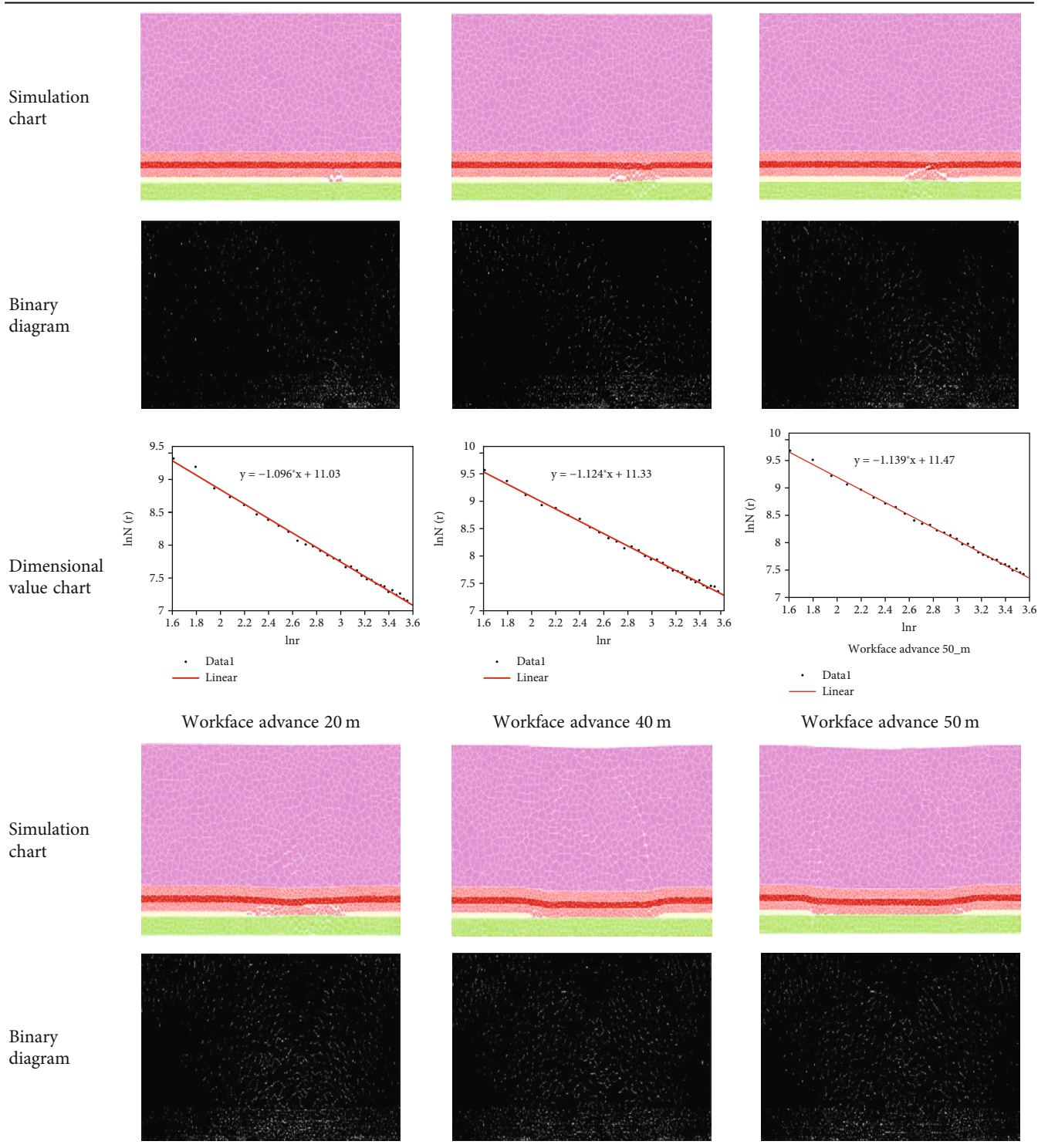


TABLE 2: Continued.

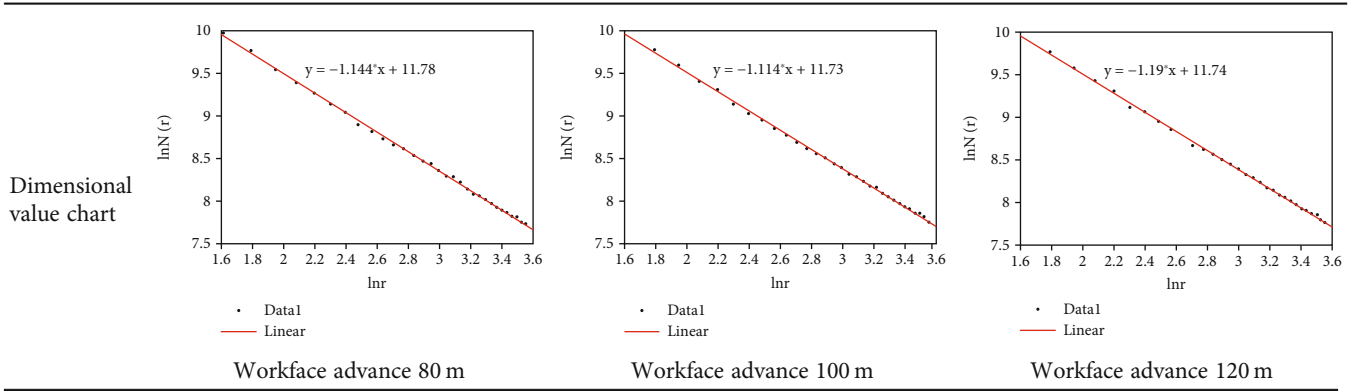


TABLE 3: Relationships between fractal dimension and overburden deformation and damage.

Propulsion distance (m)	Double logistic regression equation	Fractal dimension	Correlation coefficient	Overburden destruction stage
20	$\ln N(r) = 11.03 - 1.096 \ln(r)$	1.096	0.9963	False top collapse
40	$\ln N(r) = 11.33 - 1.124 \ln(r)$	1.124	0.9969	Direct top collapse
50	$\ln N(r) = 11.53 - 1.118 \ln(r)$	1.139	0.9982	Key layer breakage
80	$\ln N(r) = 11.78 - 1.144 \ln(r)$	1.144	0.9990	Overlying rock bending
100	$\ln N(r) = 11.73 - 1.114 \ln(r)$	1.114	0.9992	Overall collapse
120	$\ln N(r) = 11.74 - 1.119 \ln(r)$	1.119	0.9993	Collapse compaction

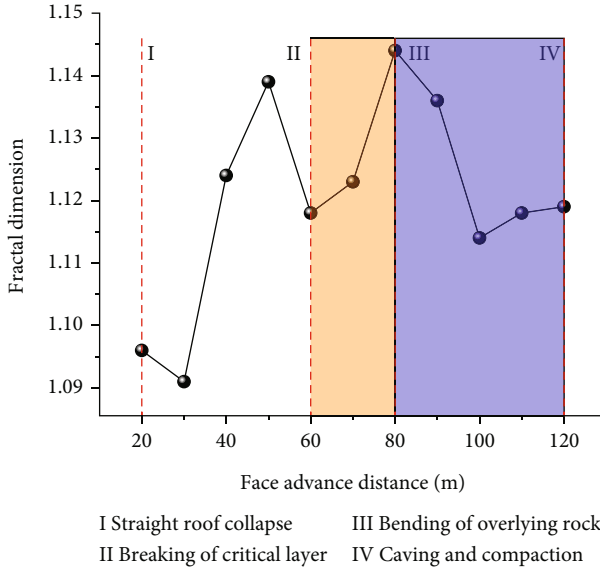


FIGURE 3: Fractal dimension of the rift network versus advance distance.

dimension, stress measurement lines were arranged in the key layer 5 m above the mined coal seam, and 12 points were taken in the stress measurement lines to observe the stress change before and after the key layer breakage in the range of 10 m to 120 m from the working face advancement, and then, the relationship between the peak stress and fractal dimension of the key layer was plotted

with the corresponding overburden fractal dimension as shown in Figure 4.

When the working face advanced to 20 m, the stress peak and fractal dimension showed a trend of gradual increase with the collapse of the pseudo-top. When the working face advances to 50 m, the key layer breaks, and the stress peak and fractal dimension increase suddenly. After the key layer is broken, the stress peak and fractal dimension drop suddenly, indicating that the lower rock layer collapses, fractures, and tends to compact. When the working face advanced to 100 m, the overburden collapsed as a whole, the stress peak reached the highest point, and the fractal dimension also rose. From this analysis, it is evident that the changes in the stress peak and fractal dimension undergo a certain synchronized rise and fall before and after breakage of the key layer.

4.3. Analysis of Overburden Energy Dissipation Characteristics. Combined with the numerical simulation, as the working face advances, the overlying rock layer in the mining area is destroyed, the overlying rock undergoes a transformation of energy, and the total energy input is changed into elastic energy and dissipation energy. From the law of thermodynamics and the energy calculation equation [28, 29], it is known that

$$U = U_e + U_d, \quad (2)$$

$$U = \int_0^e \sigma d\varepsilon, \quad (3)$$

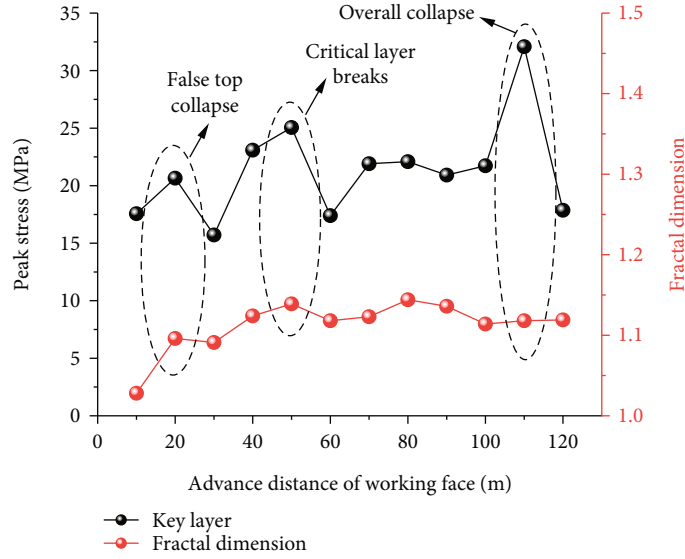


FIGURE 4: Relationship between peak stress and fractal dimension.

TABLE 4: Fracture development parameters.

Propulsion distance (m)	Fractal dimension	Critical layer stress peak (MPa)	Energy dissipation density (10^6 J/m^2)
20	1.096	20.65	15.1064
50	1.139	25.06	21.8563
80	1.144	22.09	21.6299
100	1.114	21.73	22.6979
120	1.119	17.86	13.3346

$$U_e = \frac{1}{2E} \sigma^2, \quad (4)$$

where U is the input energy per unit area, U_e is the elastic energy per unit area, U_d is the energy dissipated per unit area, ϵ is the strain of the rock, σ is the stress to which the rock is subjected, and E is the initial modulus of elasticity of the rock.

Based on the stress-strain curves of different rock seams, equations (2)–(4) were used to calculate the dissipated energy density during the deformation and damage of the overburden rock during coal seam excavation, and Table 4 lists the fracture development parameters.

The relationship curves of fractal dimension, critical layer stress peak, and dissipation energy density calculated by different advancing distances of the working face are shown in Figure 5. The overall trend of fractal dimension, peak stress in the critical layer, and dissipation energy increases and then decreases as the working surface advances. In the range of 20~80 m of the mining area, the dissipative energy density gradually increases with the increase in the advancing distance and fractal dimension, which indicates that the overburden rock is deformed and damaged and the fracture development range continues to expand dynamically. When the range of the mining area is

80~120 m, the dissipative energy density and fractal dimension show a decreasing trend, indicating that the overburden fractures are closed and gradually compacted, and the range of overburden fractures is not developing and expanding.

As shown in Figure 6, the fractal dimension versus energy fit equation is

$$D = -700.6w + 40.3w^2 - 0.8w^3 + 5.0827, \quad (5)$$

where D is the fractal dimension and w is the dissipative density. The fitting function R^2 is 0.99, which indicates a good fit. According to the curve of energy dissipation versus fractal dimension, it is known that fracture energy dissipation can be characterized by fractal dimension.

5. Fracture Field-Stress Field-Energy Field Coupling Evolution Law

5.1. Empirical Formula Used to Calculate Height of Overlying Rock Fracture Development. According to the geological conditions of the 50105 working face, the overlying rock layer of the coal seam is mainly composed of pulverized clay containing debris, and the overlying rock is soft. According to the “three lower coal mining regulations” [30], the development height of the overburden rock fissure in the soft rock layer can be calculated using the formula:

$$H = 10M + 10, \quad (6)$$

where H is the maximum height of the overburden fissure development (m) and M is the thickness of the mined coal seam (m).

According to the geological conditions of the 50105 working face, the average mining height is 2.91 m, and the maximum height of overlying rock fracture zone development is 39.1 m calculated by substituting into equation (6).

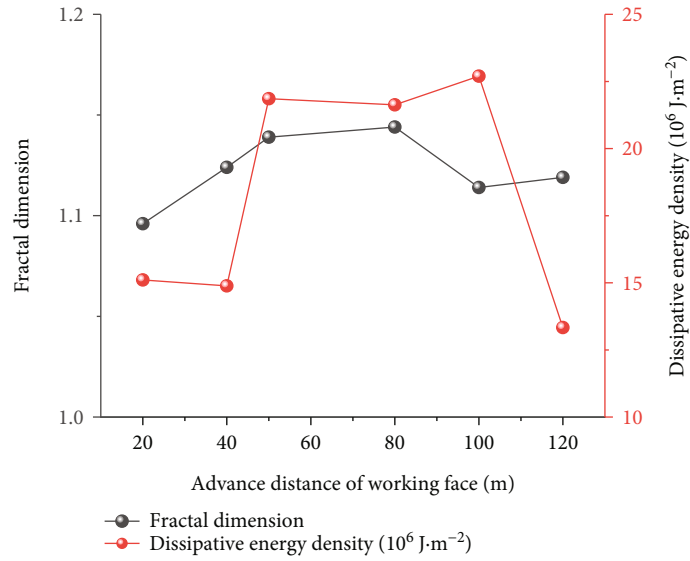


FIGURE 5: Energy versus fractal dimension curve.

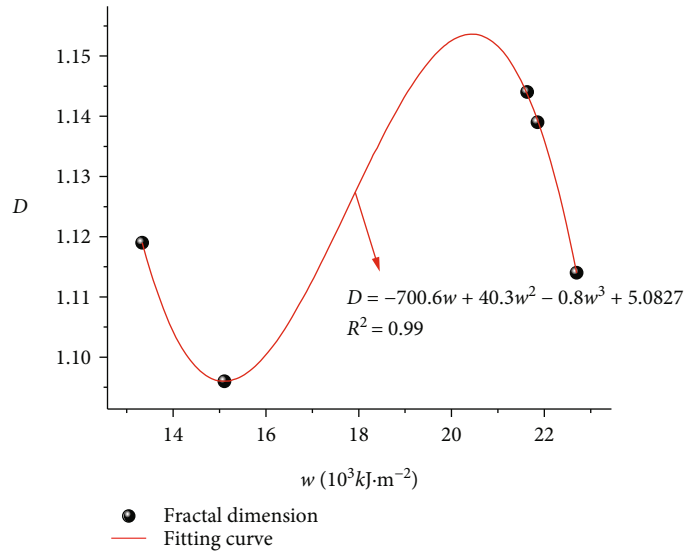


FIGURE 6: Relationship between energy and fractal dimension.

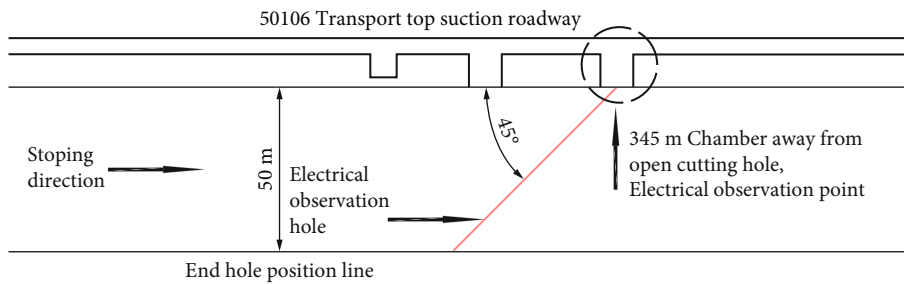


FIGURE 7: Diagram of detection holes.

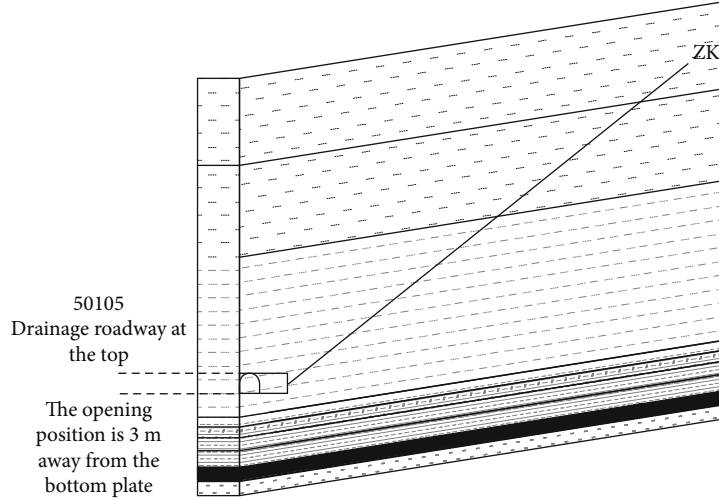


FIGURE 8: Geological section of the electrical probe hole control area.

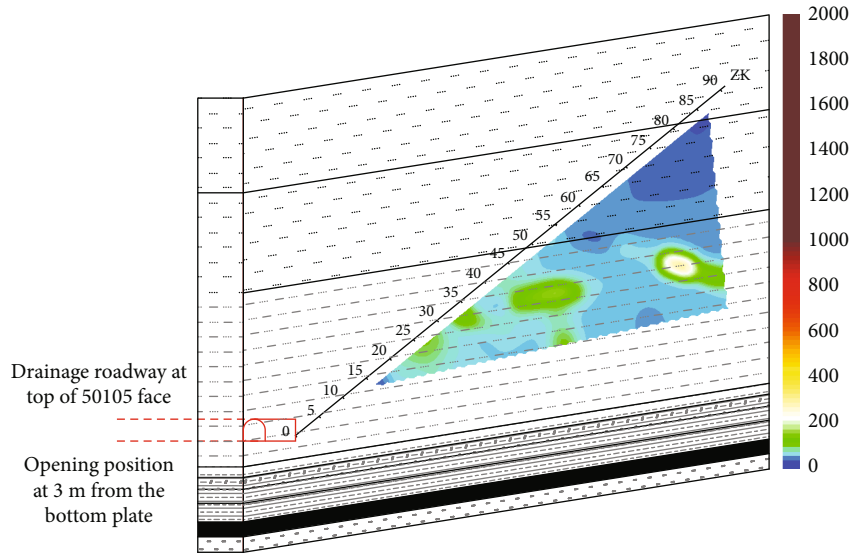


FIGURE 9: Resistivity contrast background of the 50105 working face (14 November 2019).

5.2. *Empirical Analogy Calculation Method.* Min T [31] used the least squares method to fit and calculate the development height of fissures based on actual measurement data from three mined working faces in the Panxie mine area. The empirical formula for calculating the fissure development height in the mining overburden of the Panxie mine was derived as follows:

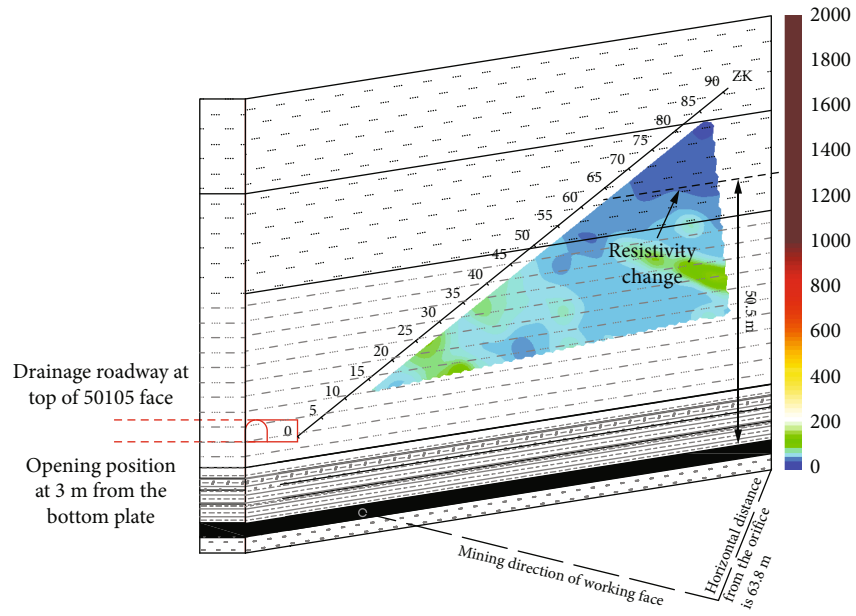
$$H = \frac{100M}{1.2M + 2.0} \pm 2.0. \quad (7)$$

The average mining height of the coal seam is 2.91 m, and the overburden fissure development height is 53.0 ± 2.0 m calculated by substituting into equation (7).

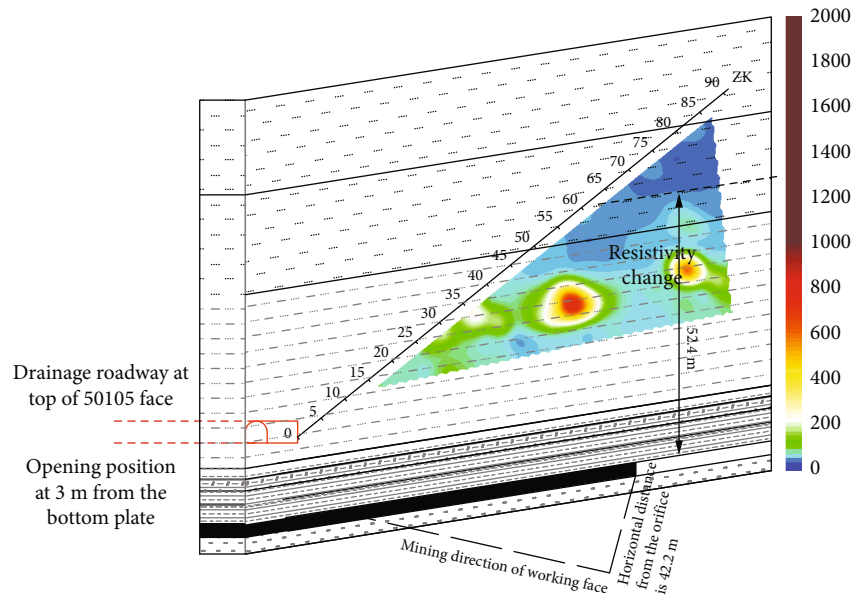
5.3. *Field Measurements of Crack Development.* To further understand the development of fractures in the overlying rock layer, based on the mining situation of the 50105 work-

ing face and existing conditions, the network parallel electric method was used to conduct observations. The network parallel electric method can be used to dynamically monitor the evolution of the overburden during the backmining period. The locations of the holes employed are shown in Figure 7.

The network parallel electrical method is used to obtain resistivity distribution maps by monitoring the differences in electrical conductivity caused by structural changes in the overlying rock layers affected by mining. After data have been obtained over a period of time, the overburden evolution phenomenon can be elucidated via a comparative analysis. The chamber at the top of the extraction lane of the transport chute was located at 345 m from the opening and used as the observation point. We designed a 39° elevation hole at a 45° angle within the construction roadway. The hole had a depth of 91 m and a control vertical height of 73 m. The number of electrodes arranged in the hole is 64, the electrode spacing is 1.4 m, electrode No. 1 is on the

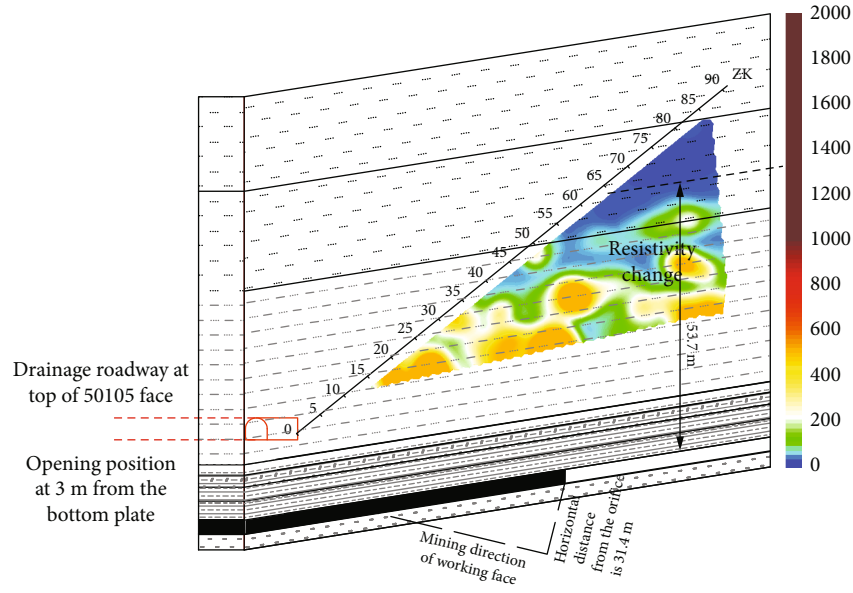


(a) November 28, 2019

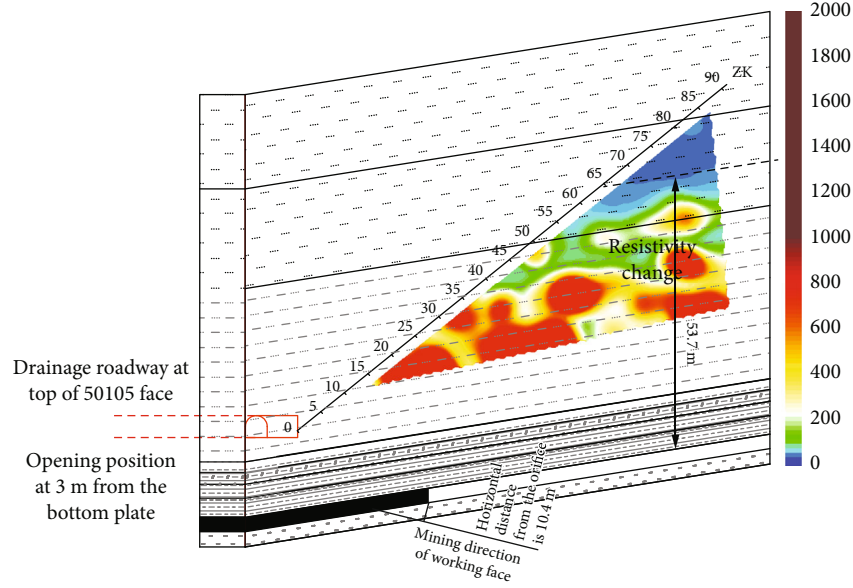


(b) December 06, 2019

FIGURE 10: Continued.



(c) December 12, 2019



(d) December 31, 2019

FIGURE 10: Resistivity observation profile of the 50105 working face.

TABLE 5: Height of overlying rock fracture development.

Working surface	Average thickness of coal seam (m)	Three lower regulations (m)	Empirical analogy (m)	Network parallel electricity method (m)
50105	3	39.1	53.0	53.7

top, and no. 64 is on the bottom, 1.0 m from the orifice. The location of the end hole is pointing in the direction of the mining area to arrange the observation system. The specific probe hole control range and geological profile are shown in Figure 8.

The observation system was installed on November 08, 2019; the first data were obtained on November 14, 2019, and the final data were collected on January 8, 2020 when the working face had advanced to the location of the hole. Figure 9 shows the resistivity profile of the working face at a distance of 97.4 m from the mouth of the hole. At this time, the overlying rock layer of the probe hole was not affected by mining and was analyzed using the background value. Figure 10(a) shows the area of local resistivity increase, at 50.5 m from the top of the coal seam. This indicates that the rock seam in this monitoring area is affected by the stress of overmining, and the internal fractures of the rock seam begin to develop. When the working face advances to within 42.2 m of the hole and enters the monitoring range, the

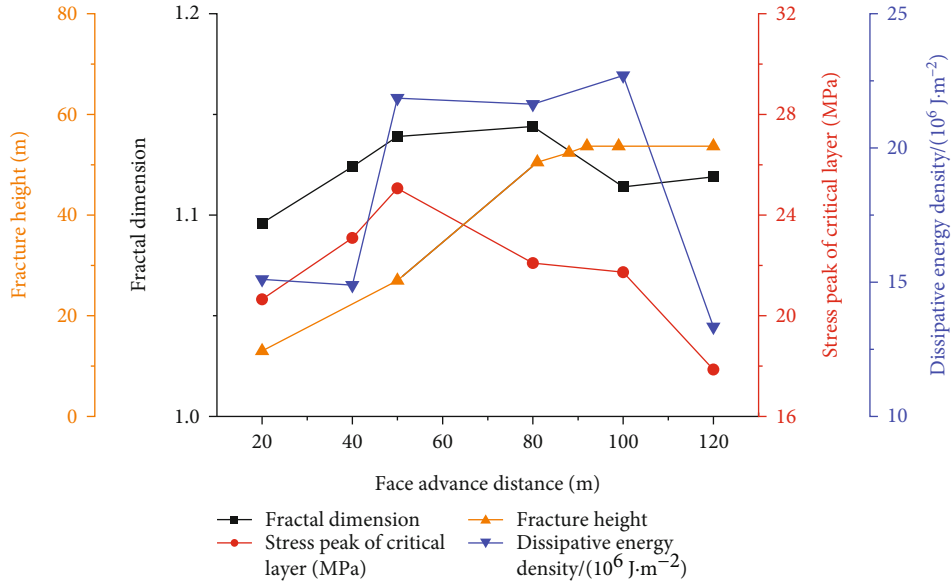


FIGURE 11: Relationship curves between key fracture field, stress field, and energy field indicators.

resistivity (shown in Figure 10(b)) appears to increase by 1.5–2.5 times overall but by approximately four times locally, and the fracture zone development height is 52.4 m. Figure 10(c) shows that the resistivity continues to increase when the working face advances to 31.4 m of the hole’s entrance, and the height of the fracture zone development is 53.7 m. A comprehensive comparison and analysis of the resistivity change values at different stages show that the fracture zone development has a height of 53.7 m.

5.4. Comprehensive Analysis of Overburden Fracture Development Height. The development height of the overburden fracture obtained by the above methods is shown in Table 5. This shows that the network parallel electricity method determines the height of the overlying fracture as 53.7 m, which is larger than the results obtained using the other two prediction methods. There is a large difference between the results obtained using the “three under the rule” and the other two methods. The literature [32] states that when the distance between the key seam and the coal seam is less than 7 to 10 times the mining height, the measured height is greater than the theoretically calculated height.

5.5. Fracture Field-Stress Field-Energy Field Coupling Analysis. In addition to the results of the numerical simulation and the network parallel electrical method observation, curves were drawn to reveal the relationships between the fracture development height, the key layer stress peak, and the dissipated energy density that reflect the fracture field, stress field, and energy field with progress in advancement of the working face (as shown in Figure 11). Figure 11 shows that the fracture development height of the soft overburden is controlled by siltstone, and it jumps step by step in relation to mining and tends to stabilize as the working face advances. However, when the key stratum is broken, there is a rapid increase in the fracture development height. The stress peak of the key stratum increases rapidly before frac-

ture and decreases gradually following fracture, and the dissipated energy density increases rapidly when the key stratum is broken and decreases rapidly after the basic roof of the goaf contacts the gangue. It can be seen that the development of the fracture field is mutually influenced and restricted by the distribution of stress and the energy fields, and no key stratum plays a decisive role owing to the relatively soft overlying strata on the 50105 working face. The main key stratum comprises siltstone (3.35 m), which has a weak control effect and a highly developed fracture zone. When the coal seam is excavated below this stratum, the mining-induced fracture field, stress field, and energy field are coupled, which affects the gas flow, subsidence, and movement of the ground strata and seriously jeopardizes safe mining. The overburden rock fracture development is inevitably accompanied by a redistribution of stress and a change in the dissipative energy density, and a stress concentration phenomenon is thus generated. The stress concentration triggers the increasing fracture development range. When fractures develop into siltstone, the lower part of the rock layer is collapsed and piled up by stress, and weak siltstone assumes almost all of the strata load. Therefore, when accumulated energy in the siltstone is released, a disaster can occur. Based on the above analysis, evolution of the process from mining to disaster associated with a soft overburden in a medium-thick coal mining seam is as follows: coal mining → stress redistribution → dissipation energy increase → fracture development → stress concentration → key stratum breaking → stress transfer → energy release → dynamic disaster.

6. Conclusions

Under the geological conditions studied in this paper, numerical simulations, fractal dimension, field measurements, and theoretical analysis were combined to comprehensively analyze the fracture development and the

multifield coupled evolutionary disaster-causing evolutionary law, as described below.

- (1) Fractal dimension of the overburden fracture tends to increase (1.096–1.139), stabilize (1.139–1.144), and then decrease (1.144–1.119) as the working face advances. The stage of increase corresponds to direct top collapse and key layer breakage, the stable stage corresponds to key layer breakage and overburden bending, and the descending stage corresponds to overburden bending, collapse, and compaction
- (2) The damage and deformation characteristics of the soft overburden of medium-thick coal seam mining are shown as follows: after the key layer is broken, the lower rock layer collapses and tends to become compacted. Bending and sinking in the upper powder clay area of the model are more obvious, and the fissures have a step shaped distribution. The trapezoidal bipedal cracks show advanced development. Overburden fractures also show dynamic development with periodic incoming pressure
- (3) According to the experimental analysis conducted using the network parallel electrical method, the overlying rock layer is affected during mining stress, which causes fissures to develop in the unmined area. With advancement of the working face, the overlying rock fissures undergo dynamic development until they stabilize at a fissure height of 53.7 m
- (4) The coupling evolution law of the weak overburden fissure field, stress field, and energy field in the medium-thick coal mining seam is as follows: coal seam mining → stress redistribution → dissipation energy increase → fissure development → stress concentration → key layer breakage → stress transfer → energy release → dynamic disaster

These results can be used as a reference for elucidating the overburden fissure development law during the management of both coal and gas extraction within the same mine.

Data Availability

The basic data supporting our research results can be found in the article.

Conflicts of Interest

The authors declare that they have no conflicts of interest.

Acknowledgments

This work was supported by the National Natural Science Foundation of China (Grant Nos. 51874107 and 52164015) and the Science and Technology Funding Projects of Guizhou Province (Grant No. 2018-5781).

References

- [1] X. L. Li, Z. Y. Cao, and Y. L. Xu, “Characteristics and trends of coal mine safety development,” *Energy Sources, Part A: Recovery, Utilization, and Environmental Effects*, vol. 2020, no. 12, pp. 1–19, 2020.
- [2] X. L. Li, S. J. Chen, E. Y. Wang, and Z. H. Li, “Rockburst mechanism in coal rock with structural surface and the microseismic (MS) and electromagnetic radiation (EMR) response,” *Engineering Failure Analysis*, vol. 124, no. 6, p. 105396, 2021.
- [3] Y. X. Zhao, C. W. Ling, B. Liu, and X. He, “Fracture evolution and energy dissipation of overlying strata in shallow-buried underground mining with ultra-high working face,” *Journal of Mining and Safety Engineering*, vol. 38, no. 1, pp. 9–18, 2021.
- [4] S. Li, C. Fan, M. Luo, Z. H. Yang, T. W. Lan, and H. F. Zhang, “Structure and deformation measurements of shallow overburden during top coal caving longwall mining,” *International Journal of Mining Science and Technology*, vol. 27, no. 6, pp. 1081–1085, 2021.
- [5] J. Wang, J. Ning, L. S. Jiang, Q. H. Gu, Q. Xu, and J. Q. Jiang, “Effect of main roof fracturing on energy evolution during the extraction of thick coal seams in deep longwall faces,” *Acta Geodynamica et Geomaterialia*, vol. 14, no. 4, pp. 377–387, 2018.
- [6] Y. K. Yang, Y. R. Ma, C. X. Ji, T. H. Kang, and X. Y. Guo, “Effect of mining thickness on overburden movement and underground pressure characteristics for extrathick coal seam by sublevel caving with high bottom cutting height,” *Advances in Civil Engineering*, vol. 2018, Article ID 6871820, 15 pages, 2018.
- [7] Y. W. Lan, R. Gao, B. Yu, and X. B. Meng, “In situ studies on the characteristics of strata structures and behaviors in mining of a thick coal seam with hard roofs,” *Energies*, vol. 11, no. 9, p. 2470, 2018.
- [8] C. Zhang, Y. X. Zhao, X. He, J. T. Guo, and Y. G. Yan, “Space-sky-surface integrated monitoring system for overburden migration regularity in shallow-buried high-intensity mining,” *Bulletin of Engineering Geology and the Environment*, vol. 80, no. 2, pp. 1403–1417, 2021.
- [9] F. Du and R. Gao, “Development patterns of fractured water-conducting zones in longwall mining of thick coal seams—a case study on safe mining under the Zhuozhang River,” *Energies*, vol. 10, no. 11, p. 1856, 2017.
- [10] D. Mondal, P. N. S. Roy, and P. K. Behera, “Use of correlation fractal dimension signatures for understanding the overlying strata dynamics in longwall coal mines,” *International Journal of Rock Mechanics and Mining Sciences*, vol. 91, pp. 210–221, 2017.
- [11] T. Liang, X. L. Liu, S. J. Wang, E. Z. Wang, and Q. S. Li, “Study on the fractal characteristics of fracture network evolution induced by mining,” *Advances in Civil Engineering*, vol. 2018, Article ID 9589364, 13 pages, 2018.
- [12] Q. L. Wu, Q. S. Wu, Y. C. Xue, P. Kong, and B. Gong, “Analysis of overlying strata movement and disaster-causing effects of coal mining face under the action of hard thick magmatic rock,” *Processes*, vol. 6, no. 9, p. 150, 2018.
- [13] L. Chen, S. W. Fan, C. Zhao, L. Zhang, and Z. H. Cheng, “Calculation method of overburden damage height based on fracture mechanics analysis of soft and hard rock layers,” *Geofluids*, vol. 2019, Article ID 3790264, 15 pages, 2019.
- [14] J. M. Shu, L. S. Jiang, P. Kong, P. Wang, and P. P. Zhang, “Numerical modeling approach on mining-induced strata

- structural behavior by considering the fracture-weakening effect on rock mass,” *Applied Sciences*, vol. 9, no. 9, p. 1832, 2019.
- [15] S. Y. Xu, Y. B. Zhang, H. Shi, Z. X. Zhang, and J. F. Chen, “Impacts of aquitard properties on an overlying unconsolidated aquifer in a mining area of the loess plateau: case study of the Changcun Colliery, Shanxi,” *Mine Water and the Environment*, vol. 39, no. 1, pp. 121–134, 2020.
- [16] L. J. Ma, B. F. Zhao, H. Wang, and Y. Gao, “Analysis of spatial differences in permeability based on sedimentary and structural features of the sandstone aquifer overlying coal seams in Western China,” *Mine Water and the Environment*, vol. 39, no. 2, pp. 229–241, 2020.
- [17] Z. H. Li, Y. K. Pang, Y. S. Bao, and Z. Y. Ma, “Research on surface failure law of working faces in large mining height and shallow buried coal seam,” *Advances in Civil Engineering*, vol. 2020, Article ID 8844249, 14 pages, 2020.
- [18] T. Hu, G. Y. Hou, S. Bu et al., “A novel approach for predicting the height of water-conducting fracture zone under the high overburden caving strength based on optimized processes,” *PRO*, vol. 8, no. 8, p. 950, 2020.
- [19] H. T. Liu, L. F. Guo, G. M. Cao et al., “Comprehensive study of strata movement behavior in mining a longwall top coal caving panel of a composite coal seam with partings,” *Applied Sciences*, vol. 10, no. 15, p. 5311, 2020.
- [20] X. He, C. Zhang, and P. H. Han, “Overburden damage degree-based optimization of high-intensity mining parameters and engineering practices in China’s western mining area,” *Geofluids*, vol. 2020, Article ID 8889663, 21 pages, 2020.
- [21] Q. Yuan, J. Chai, Y. W. Ren, and Y. L. Liu, “The characterization pattern of overburden deformation with distributed optical fiber sensing: an analogue model test and extensional analysis,” *Sensors*, vol. 20, no. 24, p. 7215, 2020.
- [22] B. B. Yang, S. C. Yuan, Y. K. Liang, and J. W. Liu, “Investigation of overburden failure characteristics due to combined mining: case study, Henan Province, China,” *Environmental Earth Sciences*, vol. 80, no. 4, p. 143, 2020.
- [23] X. H. Wang, S. Y. Zhu, H. T. Yu, and Y. X. Liu, “Comprehensive analysis control effect of faults on the height of fractured water-conducting zone in longwall mining,” *Natural Hazards*, vol. 108, no. 2, pp. 2143–2165, 2021.
- [24] W. G. Du, J. Chai, D. D. Zhang, and W. L. Lei, “Application of optical fiber sensing technology in similar model test of shallow-buried and thick coal seam mining,” *Measurement*, vol. 181, p. 109559, 2021.
- [25] C. Cheng, X. Y. Cheng, R. Yu, W. P. Yue, and C. Liu, “The law of fracture evolution of overlying strata and gas emission in goaf under the influence of mining,” *Geofluids*, vol. 2021, Article ID 2752582, 16 pages, 2021.
- [26] H. J. Fu, D. Z. Tang, T. Xu et al., “Characteristics of pore structure and fractal dimension of low-rank coal: a case study of Lower Jurassic Xishanyao coal in the southern Junggar Basin, NW China,” *Fuel*, vol. 193, pp. 254–264, 2017.
- [27] D. X. Li, E. Y. Wang, X. G. Kong, M. Ali, and D. M. Wang, “Mechanical behaviors and acoustic emission fractal characteristics of coal specimens with a pre-existing flaw of various inclinations under uniaxial compression,” *International Journal of Rock Mechanics and Mining Sciences*, vol. 116, pp. 38–51, 2019.
- [28] X. G. Kong, S. G. Li, E. Y. Wang et al., “Experimental and numerical investigations on dynamic mechanical responses and failure process of gas-bearing coal under impact load,” *Soil Dynamics and Earthquake Engineering*, vol. 142, p. 106579, 2021.
- [29] X. G. Kong, D. He, X. F. Liu et al., “Strain characteristics and energy dissipation laws of gas-bearing coal during impact fracture process,” *Energy*, vol. 242, p. 123028, 2022.
- [30] B. N. Hu, H. X. Zhang, and B. H. Shen, “Regulations of buildings, water, rail way and main well lane leaving coal pillar and press coal minin, Beijing,” *China Coal Industry Publishing House*, vol. 42, no. 1, pp. 55–56, 2017.
- [31] M. Tu, “Study on the growth height of separation fracture of mining rock in Panxie area,” *Journal of China Coal Society*, vol. 6, pp. 641–645, 2004.
- [32] J. L. Xu, X. Z. Wang, W. T. Liu, and Z. G. Wang, “Effects of primary key stratum location on height of water flowing fracture zone,” *Chinese Journal of Rock Mechanics and Engineering*, vol. 28, no. 2, pp. 381–385, 2009.